Inorg. Chem. **2006**, *45*, 7736–7747

EPR Investigation and Spectral Simulations of Iron–Catecholate Complexes and Iron–Peptide Models of Marine Adhesive Cross-Links

Jaime T. Weisser,[†] Mark J. Nilges,*[,‡] Mary J. Sever,[†] and Jonathan J. Wilker*[,†]

Department of Chemistry, Purdue University, 560 Oval Drive, West Lafayette, Indiana 47907-2084, and The Illinois EPR Research Center, 506 South Mathews Avenue, Urbana, Illinois 61801

Received April 23, 2006

Electron paramagnetic resonance (EPR) spectra are presented for iron complexes of catecholate, tironate, and a 3,4-dihydroxyphenylalanine (DOPA)-containing peptide of sequence Ac-Ala-DOPA-Thr-Pro-$CONH_2$ ("AdopaTP"). This peptide was prepared to model potential metal–protein cross-links in the adhesive used by marine mussels, *Mytilus edulis*, for affixing themselves to surfaces. Spectra are shown for iron bound to each ligand in mono, bis, and tris coordination environments. For example, the catecholate complexes {Fe(cat)}, {$Fe(cat)_2$}, and $[Fe(cat)_3]^{3-}$ are provided. Detailed simulations are presented to describe the origin of spectra for the iron–catecholate and iron–peptide species, which show that the spectral features can be accounted for only with the inclusion of *D*- and *E*-strain. The spectroscopy of each compound is shown under both anaerobic and aerobic conditions. When exposed to air, the high-spin Fe^{3+} signal of $[Fe(AdopaTP)_3]^{3-}$ decreases and an organic radical is formed. No other sample exhibited an appreciable radical signal. These data are discussed in light of the biomaterial synthesis carried out by marine mussels.

Introduction

The common blue mussel, *Mytilus edulis*, affixes itself to surfaces by generation of an impressively strong adhesive. This marine holdfast is produced by surface application of proteins containing the unusual amino acid 3,4-dihydroxyphenylalanine (DOPA, Scheme 1).[1−4] Extensive cross-linking of these DOPA-containing proteins yields the final, cured adhesive matrix.[1−4] At this time, the exact mechanism and products of these cross-linking processes remain to be identified unambiguously.

The transition metal content of mussel glues is typically elevated relative to surrounding waters. In particular, iron, zinc, and copper levels in adhesive plaques[5,6] can be well over 100 000 times that found in open seawaters.[7] Our laboratory is interested in the possibility of metal ions bringing about protein−protein cross-links. The potential for metals, in particular iron, to play a role in forming mussel glues has been proposed and explored.[8−10]

Scheme 1

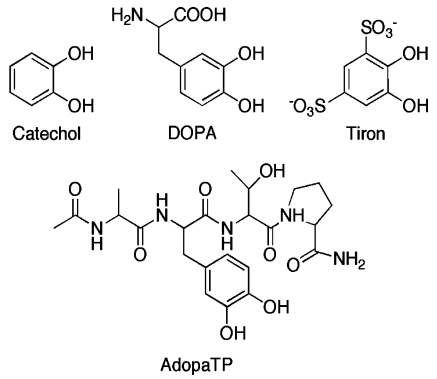

* To whom correspondence should be addressed. Email: wilker@purdue.edu
† Purdue University.
‡ The Illinois EPR Research Center.

(1) Waite, J. H.; Andersen, N. H.; Jewhurst, S.; Sun, C. *J. Adhesion* **2005**, *81*, 297−317.
(2) Waite, J. H. *Comp. Biochem. Physiol.* **1990**, *97B*, 19−29.
(3) Rzepecki, L. M.; Waite, J. H. In *Bioorganic Marine Chemistry*; Scheuer, P. J., Ed.; Springer-Verlag: New York, 1991; Vol. 4, pp 119−148.
(4) Deming, T. J. *Curr. Opin. Chem. Biol.* **1999**, *3*, 100−105.
(5) Coombs, T. L.; Keller, P. J. *Aquatic Toxicol.* **1981**, *1*, 291−300.
(6) George, S. G.; Pirie, B. J. S.; Coombs, T. L. *J. Exp. Mar. Biol.* **1976**, *23*, 71−84.
(7) Donat, J. R.; Bruland, K. W. In *Trace Elements in Natural Waters*; Salbu, B., Steinnes, E., Eds.; CRC Press: Ann Arbor, MI, 1995; pp 247−281.
(8) Taylor, S. W.; Waite, J. H.; Ross, M. M.; Shabanowitz, J.; Hunt, D. F. *J. Am. Chem. Soc.* **1994**, *116*, 10803−10804.
(9) Taylor, S. W.; Chase, D. B.; Emptage, M. H.; Nelson, M. J.; Waite, J. H. *Inorg. Chem.* **1996**, *35*, 7572−7577.

10.1021/ic060685p CCC: $33.50
Published on Web 08/25/2006

In a series of studies, we extracted the DOPA−protein precursor to adhesion from marine mussels. This adhesive precursor was reacted with various reagents in order to compare curing abilities.[11−13] Of all the biologically available metal ions examined, Fe^{3+} and Mn^{3+} brought about the greatest degrees of curing.[11,12] An electron paramagnetic resonance (EPR) spectroscopy study of intact glue produced by live mussels revealed a prominent high-spin (hs) Fe^{3+} signal and the presence of an organic radical in this material.[13] Similar hs-Fe^{3+} and radical signals were also found in a solid produced by cross-linking the DOPA-containing protein precursor of mussel glues with Fe^{3+}.[13]

To better understand the bonding and spectroscopy of marine biomaterials, we have employed comparisons with model complexes. Although interactions between iron and catechol-like ligands have been studied extensively, and to some degree by EPR spectroscopy, a systematic and descriptive EPR spectroscopic investigation has not been reported.[14−30] Herein, we present EPR spectroscopic data and simulations for iron bound to catecholate, tironate, and a DOPA-containing peptide designed to mimic mussel adhesive proteins. Each iron−ligand system is shown in the mono, bis, and tris $Fe(L)_n$ ($n = 1-3$) coordination environments, both anaerobic and aerobic. Simulated spectra show that experimentally observed differences arise from changes in the rhombic character of the zero-field tensor (D). In addition to providing comparisons for biomaterial spectroscopy, we find interesting reactivity with oxygen. The generation of organic radicals occurs only in the DOPA−peptide models, not the catecholate or tironate analogues, and only when binding iron in a tris $Fe(DOPA)_3$ coordination environment. These spectroscopic, reactivity, and simulations insights may help to understand the cross-linking processes involved in marine mussel adhesive synthesis. More broadly, this study may aid the understanding of iron interactions with other catechol-containing molecules found in siderophores,[31,32] melanin,[33,34] and the enzymatic degradation of organic compounds by enzymes such as the intradiol[35,36] and extradiol[37,38] dioxygenases.

Experimental Section

Sample Preparation. Anaerobic samples were prepared by standard Schlenk techniques under an argon atmosphere. In a typical preparation, 100 mL of water was added to a 250 mL Schlenk flask and sparged with argon for at least 30 min. Ligand was then added to the water, followed by iron(III) nitrate. Different binding modes (mono, bis, tris) were obtained by titration of metal−ligand solutions with base (NaOH). In two previous papers, we provided details on how each complex was generated in solution and assigned.[39,40] Briefly, the catecholate complexes were formed by starting with a mildly acidic 3:1 mM catechol/$Fe(NO_3)_3$ solution. Two equivalents of base (NaOH) per iron were added to maximize UV−vis spectroscopic changes ($\lambda_{max} = \sim 700$ nm), fully deprotonate one catechol, and yield the mono $[Fe(cat)]^+$ complex. Four total equivlents of base per iron deprotonated two catechols and maximized formation of bis $[Fe(cat)_2]^-$ ($\lambda_{max} = 576$ nm). Excess base (7.5 equiv) then provided the tris $[Fe(cat)_3]^{3-}$ species ($\lambda_{max} = 483$ nm). Isosbestic points showed clean conversion between discreet species. Analogous titrations were performed in reverse, starting with basic solutions of $[Fe(cat)_3]^{3-}$ and adding in acid (HCl). Identical species were observed when data were compared to the base titrations. Potentiometric titrations were also performed and, again, the same complexes were observed. Last, our data and assignments of $Fe(cat)_n$ ($n = 1-3$) are in agreement with a prior study in which these compounds were formed by base titration.[14]

Aerobic samples were prepared by two methods, both exposing anaerobic samples to air and also generating the complexes from fully aerobic solutions. More consistent results were obtained with complexes prepared from fully aerobic solutions. Thus, the aerobic samples described below are of compounds prepared in air. Base titrations of aerobic iron−ligand solutions provided UV−vis spectra with similar λ_{max} values to the analogous titrations performed anaerobically. Reverse titrations of acid (HCl) into basic solutions of $Fe(L)_3$ also yielded similar data when comparing anaerobic versus aerobic samples.

Model complexes of the ligands 1,2-dihydroxybenzene (catechol, Scheme 1), 4,5-dihydroxy-1,3-benzenedisulfonic acid (tiron, Scheme 1), and the DOPA-containing peptide Ac-Ala-DOPA-Thr-Pro-$CONH_2$ ("AdopaTP", Scheme 1), were prepared in 3:1 ratios of ligand/metal concentrations. For catechol and tiron, the ligand

(10) Frank, B. P.; Belfort, G. *Biotechnol. Prog.* **2002**, *18*, 580−586.
(11) Monahan, J.; Wilker, J. J. *Chem. Commun.* **2003**, 1672−1673.
(12) Monahan, J.; Wilker, J. J. *Langmuir* **2004**, *20*, 3724−3729.
(13) Sever, M. J.; Weisser, J. T.; Monahan, J.; Srinivasan, S.; Wilker, J. J. *Angew. Chem., Int. Ed.* **2004**, *43*, 448−450.
(14) Avdeef, A.; Sofen, S. R.; Begante, T. L.; Raymond, K. N. *J. Am. Chem. Soc.* **1978**, *100*, 5362−5370.
(15) Cox, D. D.; Que, L., Jr. *J. Am. Chem. Soc.* **1988**, *110*, 8085−8092.
(16) Cox, D. D.; Benkovic, S. J.; Bloom, L. M.; Bradley, F. C.; Nelson, M. J.; Que, L., Jr.; Wallick, D. E. *J. Am. Chem. Soc.* **1988**, *110*, 2026−2032.
(17) Galpin, J. R.; Tielens, L. G. M.; Veldink, G. A.; Vliegenthart, J. F. G.; Boldingh, J. *FEBS Lett* **1976**, *69*, 179−182.
(18) Jo, D.-H.; Chiou, Y.-M.; Que, L., Jr. *Inorg. Chem.* **2001**, *40*.
(19) Kent, T. A.; Münck, E.; Pyrz, J. W.; Widom, J.; Que, L., Jr. *Inorg. Chem.* **1987**, *26*, 1402−1408.
(20) Kita, H.; Miyake, Y.; Kamimoto, M.; Senoh, S.; Yamano, T. J. *J. Biochem.* **1969**, *66*, 45−50.
(21) Mentasti, E.; Pelizzetti, E. *J. Chem. Soc. A* **1973**, 2605−2608.
(22) Mentasti, E.; Pelizzetti, E.; Saini, G. *J. Chem. Soc. A* **1973**, 2609−2614.
(23) Nelson, M. J. *Biochemistry* **1988**, *27*, 4273−4278.
(24) Pierpont, C. G.; Lange, C. W. *Prog. Inorg. Chem.* **1994**, *41*, 331−442.
(25) Powell, H. K. J.; Taylor, M. C. *Aust. J. Chem.* **1982**, *35*, 739−756.
(26) Qian, Y.; Goodell, B.; Felix, C. C. *Chemosphere* **2002**, *48*, 21−28.
(27) Que, L., Jr.; Lauffer, R. B.; Lynch, J. B.; Murch, B. P.; Pyrz, J. W. *J. Am. Chem. Soc.* **1987**, *109*, 5381−5385.
(28) Que, L., Jr.; Kolanczyk, R. C.; White, L. S. *J. Am. Chem. Soc.* **1987**, *109*, 5373−5380.
(29) Slappendel, S.; Veldink, G. A.; Vliegenthart, J. F. G.; Aasa, R.; Malmstrom, B. G. *Biochim. Biophys. Acta* **1981**, *667*, 77−86.
(30) Taylor, S. W.; Cashion, J. D.; Brown, L. J.; Hawkins, C. J.; Hanson, G. R. *Inorg. Chem.* **1995**, *35*, 1487−1494.
(31) Raymond, K. N.; Muller, G.; Matzanke, B. F. *Top. Curr. Chem.* **1984**, *123*, 49−102.
(32) Neilands, J. B. *J. Biol. Chem.* **1995**, *270*, 26723−26726.
(33) Zecca, L.; Pietra, R.; Goj, C.; Mecacci, C.; Radice, D.; Sabbioni, E. *J. Neurochem.* **1994**, *62*, 1097−1101.
(34) Liu, Y.; Hong, L.; Kempf, V. R.; Wakamatsu, K.; Ito, S.; Simon, J. D. *Pigment Cell Res.* **2004**, *17*, 262−269.
(35) Ohlendork, D. H.; Lipscomb, J. D.; Weber, P. C. *Nature* **1988**, *336*, 403−405.
(36) Vetting, M. W.; D′Argenio, D. A.; Ornston, L. N.; Ohlendorf, D. H. *Biochemistry* **2000**, *39*, 7943−7955.
(37) Vaillancourt, F. H.; Barbosa, C. J.; Spiro, T. G.; Bolin, J. T.; Blades, M. W.; Turner, R. F. B.; Eltis, L. D. *J. Am. Chem. Soc.* **2002**, *124*, 2485−2496.
(38) Han, S.; Eltis, L. D.; Timmis, K. N.; Muchmore, S. W.; Bolin, J. T. *Science* **1995**, *270*, 976−980.
(39) Sever, M. J.; Wilker, J. J. *Dalton Trans.* **2004**, 1061−1072.
(40) Sever, M. J.; Wilker, J. J. *Dalton Trans.* **2006**, 813−822.

concentrations were 30 mM and the $Fe(NO_3)_3$ concentrations were 10 mM.[39] The AdopaTP peptide was synthesized by methods reported previously.[41] Owing to the difficulty of obtaining large quantities of peptides, the DOPA−peptide models were prepared in a 3:1 ratio with a peptide concentration of 3 mM and an $Fe(NO_3)_3$ concentration of 1 mM.[40] Our previous report discusses formation of each $\{Fe(pep)_n\}$ complex in detail.[40] For direct comparison to the peptide systems, a set of Fe−catecholate complexes were also prepared at 3 mM catechol and 1 mM $Fe(NO_3)_3$ concentrations to ensure that the behavior of the compounds did not change with concentration. No significant differences were observed when comparing the 30:10 and 3:1 mM catechol/$Fe(NO_3)_3$ systems. Glycerol was added to each sample to a final concentration of 10% to act as a glassing agent. Samples were then frozen and stored in liquid nitrogen.

Throughout this paper, metal−ligand complexes will be presented in braces to indicate that part of the coordination environment which is known. In this format {Fe(cat)}, for instance, designates one bound catecholate ligand but does not identify the remaining ligands, which are likely to be either water or hydroxide.[39] On the basis of spectroscopic titrations, complete formulations of the catecholate complexes, for example, may be $Fe(cat)(OH)(OH_2)_3$ for mono, $[Fe(cat)_2(OH)(OH_2)]^{2-}$ for bis, and $[Fe(cat)_3]^{3-}$ for tris.[39]

Instrumental Parameters. Experiments were performed on a Varian E-line Century Series EPR spectrometer with E102 microwave bridge at the University of Illinois, Urbana−Champaign. All data presented herein were taken at 15 K, unless otherwise stated. Bridge frequency was tuned to ~9.078 GHz with a microwave power of 0.2 mW. Gain settings were determined starting with the respective tris $Fe(L)_3$ complexes, with the most intense signals in the $g \approx 4.2$ region. After saturation was observed, the gain was reduced to yield full spectra. This gain setting was then used, unchanged, for the mono and bis complexes of a given ligand. The gain settings were 250 for all catecholate samples, 125 for the tironates, and 2000 for the peptide complexes. Most experiments were run with a sweep width of 4000 G, centered at 2205 G. When looking at the organic radical region, a sweep width of 2000 G, centered at 3205 G, was used. The modulation amplitude was 10 G. Where provided, resonance intensities are in arbitrary units.

Simulations. Simulation and fitting of electron paramagnetic resonance spectra used the automated simulation program SIMPIPM,[42] which is based on QPOW.[43] The spin Hamiltonian:

$$\mathbf{H} = \beta \mathbf{B}\cdot\mathbf{g}\cdot\mathbf{S} - \beta_n \mathbf{B}\cdot\mathbf{g_n}\cdot\mathbf{I} + h\mathbf{S}\cdot\mathbf{D}\cdot\mathbf{S} + h\mathbf{I}\cdot\mathbf{A}\cdot\mathbf{S}$$

is solved by exact diagonalization. Because 98% of naturally abundant Fe has no nuclear spin, the nuclear Zeeman and hyperfine terms are neglected. The spin Hamiltonian parameters are varied using the SIMPLEX method to minimize the RMS deviation between experimental and calculated spectra.[44]

The frequency-swept spectrum obtained upon diagonalization is transformed into a field-swept spectrum by iterative, Newton−Raphson solving of the eigenfield equation for each desired transition. However, iterative methods do not always converge and have trouble for nearly degenerate solutions. To improve the accuracy and speed of convergence, the DIIS (direct inversion of the iterative subspace) method of Pulay is used.[45] This method works by effectively improving the guess Hessian.

The effects of *D*-strain can be included with a joint distribution function $P(D,E)$ and performing a discrete summing or integration of possible values of D ($3/2D_{zz}$) and E ($(D_{xx} - D_{yy})/2$). As *D*-strain can be attributed to random dislocations of atoms around the metal ion center, $P(D,E)$ is usually taken as a 2-D Gaussian distribution. The contours for this 2-D error function will be ellipses. If the correlation between D and E is zero, the major and minor axes of the ellipses will lie along the D and E and $P(D,E)$ can be written as a product of two Gaussian functions. If the correlation coefficient, ϵ, is not zero, the major and minor axes will be rotated. This rotation is given by diagonalization of the error matrix R:

$$R = \begin{vmatrix} \Delta D^2 & \epsilon\sqrt{3}\Delta D\Delta E \\ \epsilon\sqrt{3}\Delta D\Delta E & \Delta E^2 \end{vmatrix}$$

Note the factor of $\sqrt{3}$ that appears because $(D^2 + 3E^2)$, not $(D^2 + E^2)$, is invariant to coordinate transformation. The vectors corresponding to the major and minor axes of the error ellipses will be

$$\dot{F} = \cos\theta\dot{D} + \sin\theta\dot{E}/\sqrt{3}$$

$$\dot{G} = \sin\theta\dot{D} + \cos\theta\dot{E}/\sqrt{3}$$

where

$$\tan 2\theta = \frac{2R_{12}}{R_{22} - R_{11}}$$

The length and width of the ellipse corresponding to $P = 1/2$ are

$$\Delta F = (\cos^2\theta R_{11} + \sin^2\theta R_{22} + 2\cos\theta\sin\theta r_{12})^{1/2}/2$$

$$\Delta G = (\cos^2\theta r_{22} + \sin^2\theta R_{11} - 2\cos\theta\sin\theta r_{12})^{1/2}/2$$

Transforming $P(D,E)$ to the system where R is diagonal gives a distribution function, $P(F,G)$, which can be represented as the product of two uncorrelated Gaussians:

$$P(F,G) = \frac{\ln 2\sqrt{\ln 2/\pi}}{\Delta F\Delta G}\exp\left(-\frac{\ln 2(F - F_0)^2}{\Delta F^2}\right)\exp\left(-\frac{\ln 2(G - G_0)^2}{\Delta G^2}\right)$$

Where ΔF or ΔG represent the half-width at half-height of their respective distributions. Note that, if ϵ is equal to one, either ΔF or ΔG is zero and $P(F,G)$ reduces to a single Gaussian.

Because integration of F and G is accounted for by discrete summing of spectra over a large number of possible values, computational times are long and spectra show noise or graining due to the finite stepping of values for F and G.[46] If the variances in D and E are small, the effect of *D*-strain can be accounted for by using a Gaussian line width that is proportional to the dispersion of the spin Hamiltonian with respect to the strained variable, i.e., the partial gradient of the energy. SIMPIPM can calculate this Gaussian broadening analytically, and this gradient method can reproduce very well the variation in line width for discrete transitions.[47,48] However, for the systems studied here, the strain in D is on the same order of D itself; such calculations will not accurately reproduce the overall spectral line shape when individual transitions

(41) Sever, M. J.; Wilker, J. J. *Tetrahedron* **2001**, *57*, 6139−6146.
(42) Nilges, M. J. *SIMPIM*; University of Illinois: Urbana−Champaign, 2002.
(43) Nilges, M. J. Thesis, University of Illinois, Urbana−Champaign, 1979.
(44) Mattson, K. Thesis, University of Illinois, Urbana−Champaign, 1991.
(45) Pulay, P. *Chem. Phys. Lett.* **1980**, *73*, 393−398.
(46) Yahiaoui, E. M.; Berger, R.; Servant, Y.; Kliava, J.; Cugunov, L.; Mednis, A. *J. Phys. Condens. Matter* **1994**, *6*, 9415−9428.
(47) Nilges, M. J.; Belford, R. L.; Francesconi, L. C. *Simulation of Strain in EPR Spectra Using Methods of Gradients*; 40th Rocky Mountain Conference on Analytical Chemistry: Denver, 1998.
(48) Rahimi-Moghaddam, P.; Upadrashta, Y.; Nilges, M. J.; Weil, J. A. *Appl. Magn. Res.* **2003**, *24*, 113−125.

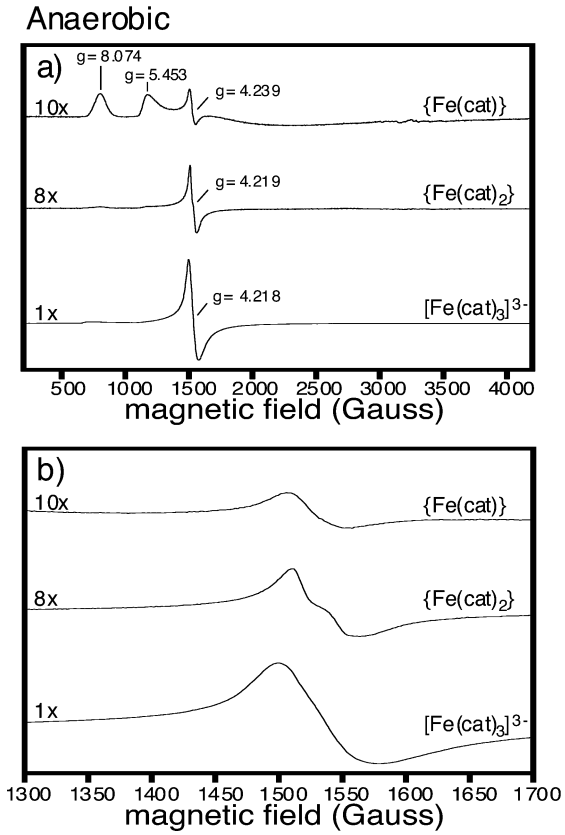

Figure 1. EPR spectra of anaerobic iron(III) catecholate complexes of (a**)** the full spectral region and (b**)** an expansion of the $g \approx 4.2$ signal only. The vertical scales of each spectrum are adjusted as labeled to allow comparisons. Here the spectrum of the mono species is expanded 10-fold vertically relative to the tris complex. The bis compound is expanded 8-fold relative to $[Fe(cat)_3]^{3-}$.

collapse into a non-Gaussian line shape. To reproduce the line shape accurately and eliminate the graining due to the summing over finite values of F and G, we have used a hybrid method. Because the distribution in F and G is Gaussian, we can calculate the strain in F and G as a convolution of two Gaussians, one that is large and calculated by discrete summing and the other that is smaller and incorporated in the line width calculated by the gradient method.

$$\Delta F^2_{\text{tot}} = \Delta F^2_{\text{discrete}} + \Delta F^2_{\text{gradient}}$$

The ratio of the splitting into discrete and gradient components is optimized to give the best compromise between spectral fidelity and noise/graining.

Results

Spectra of Anaerobic {Fe(cat)$_n$} ($n = 1-3$) Catecholate Complexes. {Fe(cat)}. In the case of iron(III) monocatecholate, {Fe(cat)}, several features were observed which are similar to those when iron is chelated with catechol and catechol-like ligands.[16] As can be seen in Figure 1a, a pair of well-defined features were found at $g = 8.10$ and 5.45, as well as a broader feature around $g \approx 3.2-2.6$. High-spin iron(III) centers with an intermediate rhombic character ($E/D \approx 0.1-0.15$) often give rise to signals of this nature.[16,17,19,49−52] In addition to these resonances was an isotropic but somewhat asymmetric feature at $g = 4.24$ similar to that typically found for hs-Fe^{3+} in a completely rhombic environment ($E/D = 1/3$).[16,17,20,23,29,49−52] A set of weak peaks in the region from $g \approx 2.2$ to $g \approx 1.9$ was just discernible above the noise level. With an apparent splitting of around 90 G, these features are most likely due to Mn(II). The appearance of a $g = 4.3$ peak in addition to the peaks at $g = 8$, 5, and 3 could suggest that there may be the presence of more that one type of metal center.[16]

We point out a marked similarity between the EPR spectra of {Fe(cat)} and another iron-catecholate complex, [Fe(HDA)(DBC)]$^{2-}$, prepared to mimic an enzyme active site.[16] The coordination environment of [Fe(HDA)(DBC)]$^{2-}$ is comprised of the two oxygens of 3,5-di-*tert*-butylcatecholate (DBC) and the donors of the HDA ligand: two carboxylates, one phenolate, and one amine.[16] Given that an iron coordination environment comprised of predominantly oxygen donors has been shown previously to provide a similar spectrum, we conclude that the coordination environment of {Fe(cat)} contains the two catecholate oxygens, as well as the oxygens of water or hydroxide ligands to complete the coordination sphere.

{Fe(cat)$_2$}. Iron(III) bis-catecholate, {Fe(cat)$_2$}, exhibited a spectrum that appeared quite different from that of the mono counterpart (Figure 1a). The rhombic $g = 4.22$ signal now dominates the spectrum, but in the low-field wing, a pair of features at $g \approx 8.1$ and 5.5 can still be distinguished. Closer examination of the $g = 4.22$ signal showed a distinct splitting (Figure 1b). Unlike {Fe(cat)}, no other features were apparent in regions of the spectrum beyond that of $g \approx 4.3$ in the {Fe(cat)$_2$} sample. Like the {Fe(cat)} spectrum, the appearance of peaks at $g \approx 8$ and 5, in addition to the $g \approx 4.3$ peak in the spectrum of {Fe(cat)$_2$}, suggests that there may be two components present.

[Fe(cat)$_3$]$^{3-}$. Figure 1a shows that the spectrum of iron(III) catecholate in the tris coordination environment, $[Fe(cat)_3]^{3-}$, is typical of completely rhombic ($E/D = 1/3$) hs-Fe^{3+}. In addition to the nearly isotropic though somewhat asymmetric $g = 4.22$ signal, which arises from the middle Kramer's doublet, we observed an edge in the low-field wing of the $g = 4.22$ signal at $g \approx 9.6$. This signal at $g \approx 9.6$ arises from the two other Kramer's doublets, which unlike the middle doublet, give rise to rather anisotropic features. There was no observable evidence of splitting in the $g = 4.22$ signal of the tris environment, as opposed to that present in the bis environment.

Simulations of Anaerobic {Fe(cat)$_n$} ($n = 1-3$) Catecholate Spectra. The differences in EPR spectra observed for iron−catecholate complexes can be ascribed primarily to differences in the rhombic character of the zero-field tensor, D. The spectra are typical of high-spin iron(III) for which the magnitude of the zero-field tensor, $D(1 + 3\lambda^2)^{1/2}/h$ ($\lambda = E/D$) is larger than the microwave frequency, ν. In

(49) Aasa, R. *J. Chem. Phys.* **1970**, *52*, 3919−3930.
(50) Chen, C.-H.; Lee, Y.-Y.; Liau, B. C.; Elango, S.; Chen, J. H.; Hsieh, H.-Y.; Liao, F.-L.; Wang, S.-L.; Hwang, L.-P. *J. Chem. Soc., Dalton Trans.* **2002**.
(51) Palmer, G. *Biochem. Soc. Trans.* **1985**, *13*, 548−560.
(52) Simaan, A. J.; Banse, F.; Girerd, J.-J.; Wieghardt, K.; Bill, E. *Inorg. Chem.* **2001**, *40*, 6538−6540.

this low-field limit, the energy levels can be described by three doubly degenerate Kramer's doublets each having an effective spin of 1/2.[49,53] If the zero-splitting is larger than the microwave energy, transitions between the three doublets cannot occur.

If the temperature is larger than D/k, transitions involving all three doublets can occur. However, in most cases, only one or maybe two of the Kramer's doublets are readily observed in the EPR spectrum. For the case of axial symmetry with $\lambda = 0$, only the lowest doublet with effective g values of $g = 6$ and $g_\perp = 2$ is observed (assuming the true g value of 2 and $D > 0$; for $D < 0$, the ordering of the three doublets is reversed). The other two doublets have effective g principal values of $g = 6$ and $g_\perp = 0$ and $g = 10$ and $g_\perp = 0$.[49,53] Because the intensity of the first-derivative spectrum will vary as the inverse square of the spectral width, these two highly anisotropic doublets will have an extremely small intensity. In the case of rhombic symmetry, $\lambda = 1/3$, there is one doublet, the middle one, which will have an isotropic g of 4.29. The lower and upper doublets are anisotropic with values of g_x, g_y, and g_z at 0.86, 0.61, and 9.68 and 0.86, 9.68, and 0.61, respectively. Again, because the spectral width of the anisotropic doublets is much greater than that of the isotropic $g = 4.3$ doublet, usually only the $g = 4.3$ feature is readily observed. For symmetry between axial and rhombic symmetry, it is possible to observe features from both the low and middle doublets.

In the low-field limit, the EPR spectrum depends only upon the asymmetry parameter, λ, and is independent of the value of D. If the value of D/h is close to the microwave frequency, the effective g values will show a second-order shift proportional to the ratio of the microwave energy to the value of D. The effective g values will also depend slightly upon the principal values of the true g matrix. If the value of D is further decreased, one approaches the high-field limit where $D \ll h\nu$. Here there are five putatively allowed transitions. The $m_s = -1/2$ to 1/2 will be at $g = 2$ (or the true g value), while the other four, $m_s = -5/2$ to $-3/2$, $m_s = -3/2$ to $-1/2$, $m_s = 1/2$ to 3/2, and $m_s = 3/2$ to 5/2 transitions, will be distributed around $g = 2$. The spacing of the multiplet pattern around $g = 2$ is now dependent upon D to the first order.

The ability to observe spectral features also depends on D-strain. In general, there is a random spread of D and E values which arise from random distortions of ligand geometry around the iron atom. For metal complexes in solution, this is often attributable to hydrogen bonding of the solvent to the metal or ligand atoms and/or poor glassing of the solvent when the sample is frozen. The effect of D-strain will be to broaden features, particularly those for which their values of g_{eff} are sensitive to the value of D and E. In the low-field limit, the spectra are dependent primarily on the asymmetry parameter, $\lambda = E/D$, and as such, line broadening of a specific feature will depend primarily on its sensitivity to E/D rather than D. Because different features show differing sensitivity to the values of D and E, the overall shape of the spectrum can be highly dependent upon D-strain and unless D-strain is considered, a proper analysis of the spectrum cannot be made.

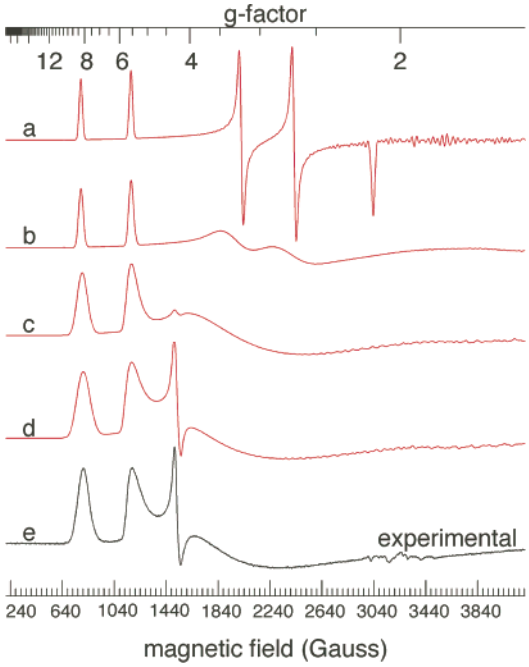

Figure 2. Simulated and experimental spectra of {Fe(cat)}. (a−d) Simulated spectra with varying amounts of strain; remaining parameters as listed in Table 1. (a) No strain in D or E. (b) $\Delta D = 0.048$ cm^{-1} $\Delta E = 0.005$ cm^{-1}. (c) $\Delta D = 0.143$ cm^{-1} $\Delta E = 0.015$ cm^{-1}. (d). Best fit; $\Delta D = 0.191$ cm^{-1} $\Delta E = 0.019$ cm^{-1}. (e) Experimental.

{**Fe(cat)**}**.** The EPR spectrum of the 1:1 complex of iron and catecholate (Figure 1a) gives rise to features that can be interpreted at first sight to have an D tensor with a intermediate value of λ around 0.1 and a second component with $\lambda = 1/3$ ($g = 4.3$). The simulated features at $g = 8.10$ and 5.52 (Figure 2) are due to the g_y feature for the middle doublet and g_z feature of the lowest doublet, respectively. The g_x and g_z features of the middle doublet and the g_x and g_y features of the lowest doublet are not resolved due to D-strain. The effect of D-strain upon the spectrum is shown in the simulations of Figure 2. For the top spectrum with no strain (Figure 2a), three of the other four features are visible (the fourth feature at $g = 1.52$ is just out of spectral range). When D-strain is included (Figure 2b), the feature at $g = 2.14$ is completely washed out and the two features at $g = 2.67$ and 3.22 are heavily broadened but still resolved. To a first approximation, the smaller the effective g value, the greater will be the line broadening. As the D-strain is increased (Figure 2c and d) the high-field part of the EPR spectrum for the two doublets collapses to a single broad (1200 G peak to peak) line at about $g = 3.5$ and only the two low field components are resolved. In addition, a peak at $g = 4.3$ grows in. This peak appears because the distribution of D and E will give rise to the possibility of sites having $\lambda = 1/3$ ($g = 4.3$), as well as sites having a broad range of other values of λ. Though the $g = 4.3$ peak represents only a small fraction of sites, it is relatively intense since at $\lambda = 1/3$ the anisotropy for the middle doublet completely collapses. The simulations clearly show that, in order

(53) Wickham, H. H.; Klein, M. P.; Shirley, D. A. *J. Chem. Phys.* **1965**, *42*, 2113-2117.

Table 1. EPR Simulation Parameters for {Fe(cat)$_n$} and {Fe(pep)$_n$}

	D_0 (cm^{-1})	E_0 (cm^{-1})	λ	ΔD (cm^{-1})	ΔE (cm^{-1})	ϵ	g_{iso}	W_r (Gauss)
Fe(cat)	0.817	0.098	0.120	0.191	0.019	−0.675	1.997	24.0
Fe(cat)$_2$	0.421	0.104	0.247	0.324	0.018	−0.925	1.989	12.1
Fe(cat)$_3$	0.319	0.095	0.299	0.135	0.030	−0.638	1.992	35.1
Fe(pep)[a]	0.157	0.023	0.146	0.163	0.010	0.186	1.991	42.4
	0.440	0.105	0.243	0.341	0.037	−0.016	1.981	22.0
Fe(pep)$_2$[b]	0.427	0.106	0.248	0.326	0.016	−0.921	1.983	12.4
	0.138	0.021	0.155	0.102	0.009	0.0	1.984	40.6
Fe(pep)$_3$	0.312	0.098	0.313	0.130	0.041	−0.362	1.984	26.2

[a] Two components or double distribution. Ratio of components is 4.3:1. [b] Two components or double distribution. Ratio of components is 4.4:1

to fit the experimental spectrum, particularly the width and position of the broad peak at $g = 3.5$, a relatively significant D-strain ($\Delta D/D_0 = 0.23$; $\Delta E/E_0 = 0.20$) has to be included and that such D-strain is large enough to produce a $g = 4.3$ peak.

Parameters used in the simulation of the spectrum of {Fe(cat)} are listed in Table 1. Because we are near the low-field limit where the spectrum depends primarily on E_0/D_0, $\Delta D/D$, and $\Delta E/E$, the accuracies of the values of D_0, E_0, ΔD, and ΔE are limited, and the values determined for D_0 and E_0 probably represent lower limits. The sign of D and E is indeterminate. To obtain more accurate values of D_0 and E_0, as well as their sign, other experiments (higher frequency and/or lower temperature) would be needed.

{Fe(cat)$_2$}. From a first look the spectrum of {Fe(cat)$_2$}, which is dominated by a peak at $g = 4.3$, we might assign the spectrum to a rhombic system with $\lambda = 1/3$ (Figure 1). However, close inspection and simulation show this initial analysis is not the case (Figure 3). Not only are there wings on the $g = 4.3$ signal extending out 500 G or so, but there are a low field peak at $g = 8.1$ and a sharp shoulder at $g = 5.5$. Even though the two anisotropic doublets for $\lambda = 1/3$ are expected to give rise to a very weak feature at $g = 9.6$, we find something different. Instead, the features at $g = 8.1$ and 5.5 are those that are expected when λ is in the ranges of 0.10−0.15. As such, on second sight, one may consider this spectrum as being due to two species, one with $\lambda = 1/3$ and another with λ around 0.12. Simulations of the spectrum show something different (Figure 3). Rather, a single species with a median value of $\lambda = 0.25$ and a very large strain in D ($\Delta D/D_0 = 0.77$; $\Delta E/E_0 = 0.17$) will reproduce the spectrum. Also noticeable under closer inspection is the 25 G splitting of the $g = 4.3$ peak. If D is in the low-field limit, as λ approaches the value of 1/3, the x, y, and z components of the middle doublet collapse to a single peak. If $D[(1 + 3\lambda^2)]^{1/2}/h$ is decreased away from the low-field limit, two principal values of the effective g matrix will start to move toward the true g value faster than the third one, resulting in a splitting of the line. The net effect is that the sharp peak at $g = 4.3$ will be diminished and sites with small values of D, which are more readily split, are more pronounced in the spectrum. The observed splitting, which is found to be dependent upon D and λ, can be used to approximate the value of D. The splitting of the $g = 4.3$ line will also be dependent upon the anisotropy of the true g matrix and the quartic splittings a and F.[54] In our simulations, we have assumed that the anisotropy in the true g matrix, as well as the values of a and F, are zero. Although these terms are small, the inability to determine them independently limits the accuracy of the values of D and E obtained from the simulations.

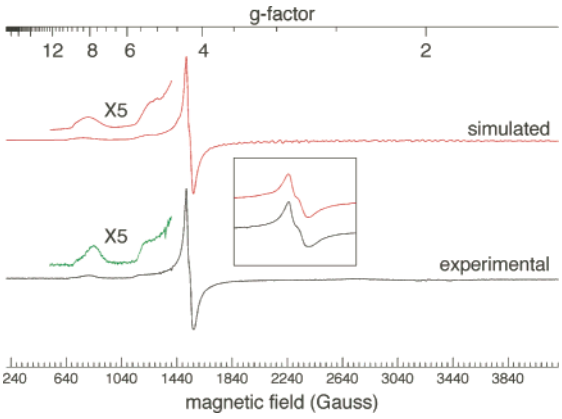

Figure 3. Simulated and experimental spectra of {Fe(cat)$_2$}. Inset shows $g = 4$ region at higher resolution.

In our initial report on EPR spectra of mussel adhesive plaques, protein, and models, we found this splitting of the $g = 4.3$ signal for bis complexes.[13] We used this splitting to help distinguish bis coordination from mono and tris, in which no splitting was observed. These simulations show that, indeed, splitting at $g = 4.3$ appears to be characteristic for iron bound by two catecholates. Consequently, this spectral feature may prove to be useful for future studies in which EPR spectroscopy is used to identify the coordination environment of iron in biological samples.

[Fe(cat)$_3$]$^{3-}$. The spectrum of [Fe(cat)$_3$]$^{3-}$ consists of a peak at $g = 4.3$ and a peak at $g = 9.6$ (Figure 1). Both peaks can be assigned to sites with $\lambda = 1/3$. However, to reproduce the wings about the $g = 4.3$ feature and the wing extending from the $g = 9.6$ feature to higher fields, considerable D-strain must be included ($\Delta D/D_0 = 0.42$; $\Delta E/E_0 = 0.32$, Figure 4). The median value of $\lambda = 0.30$ is close to 1/3. Similar spectra have been observed for iron in borate glasses, and such spectra have been interpreted in terms of D-strain.[46,55] While the $g = 4.3$ feature shows distinct asymmetric line shape, there is no splitting as is seen in the 1:2 complex. This occurs for two reasons. First, the median value of λ is much closer to 1/3, and as such, there are more sites having conditions necessary for an isotropic or nearly isotropic g matrix, that is, $\lambda = 1/3$ and D in the low-field

(54) Golding, R. M.; Kestigian, M.; Tennant, C. W. *J. Phys. C: Solid State Phys.* **1978**, *11*, 5041−5049.
(55) Berger, R.; Kliava, J.; Yahiaoui, E.-M.; Bissey, J.-C.; Zinsou, P. K.; Beziade, P. *J. Non-Cryst. Solids* **1995**, *180*, 151−163.

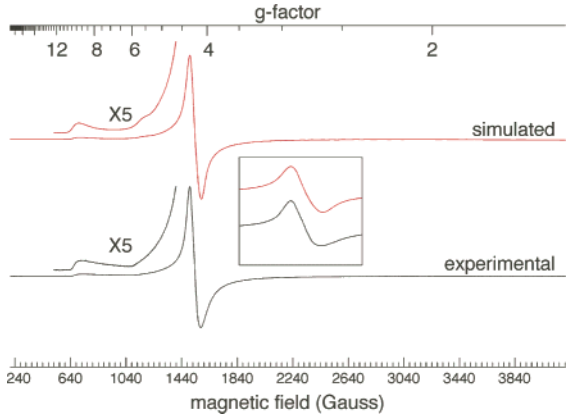

Figure 4. Simulated and experimental spectra of $[Fe(cat)_3]^{3-}$. Inset shows $g = 4$ region at higher resolution.

limit. Second, the distribution in D and E is not as well correlated as that for the 2:1 complex, which decreases resolution. The values of $D_0 = 0.32$ cm^{-1} and $\lambda = 0.31$ are fairly typical for tris chelation to oxygen or nitrogen bidentate ligands to iron.[56,57]

Reviewing the simulation parameters in Table 1, the most visible trend is that of the increase in the median value of λ as the number of coordinated catecholates increases. The $[Fe(cat)_3]^{3-}$ complex is expected to have a trigonally distorted octahedral geometry for which the median value of $\lambda = 0.31$ is quite reasonable. Unlike the tris coordinated complex, the mono and bis complexes require the coordination of water or buffer molecules to complete the coordination sphere. As such, there should be a definite axial component to the ligand field around the iron atom, particularly for the mono complex where a strong axial component is expected along the bisector through the two oxygen−iron bonds of the metal−ligand complex. While the accuracy of the absolute values of D_0 and E_0 is limited, it is seen that the value of E_0 is roughly the same for all three catecholate complexes and the value of D_0 is found to decrease with increasing coordination number. This is consistent with the picture of the bis and especially the mono complex having a strong axial ligand field component as a result of the catecholate ligand(s) not forming a complete coordination sphere.

Spectra of Anaerobic {Fe(tiron)$_n$} ($n = 1-3$) Tironate Complexes. {Fe(tiron)}. The mono-tironate complex, {Fe(tiron)}, displayed a spectrum quite similar to that of {Fe(cat)}, as shown in Figure 5a. The well-defined hs-Fe^{3+} features are seen at $g = 8.10$, 5.44, and 4.26, as well as the broad feature around $g = 3$. Unlike the analogous {Fe(cat)}, no extra features were apparent in later regions of the spectrum of {Fe(tiron)}.

{Fe(tiron)$_2$}. The iron(III) bis-tironate, $\{Fe(tiron)_2\}$ (Figure 5a), appeared similar to $\{Fe(cat)_2\}$ (Figure 1a). Again, a very weak hs-Fe^{3+} feature is seen near $g \approx 8.1$, as well as the strong resonance centered at $g = 4.22$ (Figure 5b). The bis complex showed more spectral intensity at $g = 4.22$ compared to the mono species, indicating an increase in

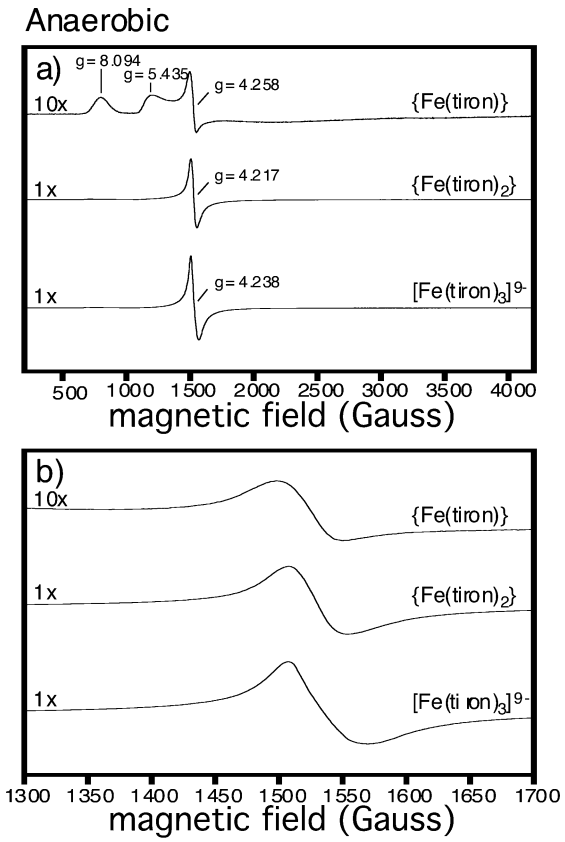

Figure 5. EPR spectra of anaerobic iron(III)−tironate complexes of (a) the full spectral region and (b) an expansion of the $g \approx 4.2$ signal only. The vertical scales of each spectrum are adjusted as labeled to allow comparisons.

rhombic character.[51] Figure 5b displays an expanded view of this spectral region, yet does not show signs of splitting in {Fe(tiron)$_2$} like that seen in {Fe(cat)$_2$}. A spectrum of this same sample obtained at a temperature of 77 K (data not shown), rather than the 15 K used for all spectra shown here, exhibited clear splitting similar to that seen for {Fe(cat)$_2$}.

[Fe(tiron)$_3$]$^{9-}$. The EPR spectrum of $[Fe(tiron)_3]^{9-}$, like that of $[Fe(cat)_3]^{3-}$, was dominated by a $g = 4.24$ hs-Fe^{3+} feature (Figure 5a). Unlike $[Fe(cat)_3]^{3-}$, the $[Fe(tiron)_3]^{9-}$ spectrum was more symmetrical than either the mono or bis compounds. Similar to the spectrum of $[Fe(cat)_3]^{3-}$, we found no evidence of splitting in the center of the signal and observed a flat baseline.

Spectra of Anaerobic {Fe(pep)$_n$} ($n = 1-3$) Peptide Complexes. After studying the EPR spectra of catecholate and tironate complexes, we move to iron complexes of a DOPA-containing peptide. The peptide examined here is of sequence Ac-Ala-DOPA-Thr-Pro-$CONH_2$ (AdopaTP), chosen to represent the amino acid composition of Mefp-3, a protein employed by marine mussels in adhesive synthesis.[4,58−61] This peptide was synthesized by our methods pub-

(56) Biaso, F.; Duboc, C.; Barbara, B.; Serratrice, G.; Thomas, F.; Charapoff, D.; Beguin, C. *Eur. J. Inorg. Chem.* **2005**, 467−478.
(57) Collison, D.; Powell, A. K. *Inorg. Chem.* **1990**, *29*, 4735.
(58) Warner, S. C.; Waite, J. H. *Marine Biol.* **1999**, *134*, 729−734.
(59) Vreeland, V.; Waite, J. H.; Epstein, L. *J. Phycol.* **1998**, *34*, 1−8.
(60) Papov, V. V.; Diamond, T. V.; Biemann, K.; Waite, J. H. *J. Biol. Chem.* **1995**, *270*, 20183−20192.
(61) Rzepecki, L. M.; Chin, S.-S.; Waite, J. H.; Lavin, M. F. *Mol. Marine Biol. Biotech.* **1991**, *1*, 78−88.

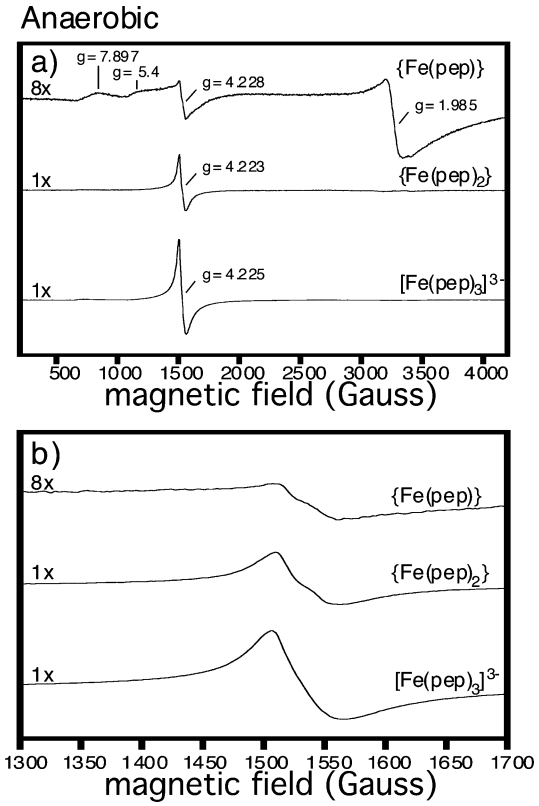

Figure 6. EPR spectra of anaerobic iron(III) AdopaTP complexes of (a) the full spectral region and (b) an expansion of the $g \approx 4.2$ signal only. The vertical scales of each spectrum are adjusted as labeled to allow comparisons.

lished previously.[41] Note that the N-terminus of the peptide was acetylated and the C-terminal acid was changed to an amide. These modifications were made to prevent metal binding from the termini and to focus chemistry on the amino acid side chains. Since it is known that DOPA is necessary for cross-linking and adhesion to occur in mussel adhesives,[4,61,62] such models should give us a better indication of potential iron-binding modes in mussel adhesives. These spectra can be compared to those taken of the marine biomaterial.[13]

{Fe(pep)}. A spectrum of iron(III) mono-peptide, {Fe(pep)}, contained several noticeable differences in comparison to the catecholate and tironate model analogues, as shown in Figure 6a. The pair of features at $g = 8.10$ and 5.45 in the catecholate complex were replaced with broader features at $g = 7.90$ and $g \approx 5.4$. Also seen is a rhombic hs-Fe^{3+} signal centered at $g = 4.23$, a value comparable to other Fe−DOPA complexes.[9,63,64] A small degree of splitting was observable in this somewhat asymmetrical resonance. A major distinction between this {Fe(pep)} spectrum and those of {Fe(cat)} and {Fe(tiron)} was the occurrence of an intense, highly unsymmetrical signal centered at $g = 1.985$. Such a signal may arise from either hs-Fe^{3+}, low-spin Fe^{3+}, or iron−iron coupling.[9,52,65−67]

{Fe(pep)$_2$}. As shown in Figure 6a, iron(III) bis-peptide, {Fe(pep)$_2$}, exhibited a spectrum similar to those of the {Fe(cat)$_2$} and {Fe(tiron)$_2$} complexes, with a typical rhombic hs-Fe^{3+} signal, centered at $g = 4.22$, with a wing stretching down to a broad peak $g \approx 8$. The $g = 4.22$ signal was found to be both more intense and narrower than in {Fe(pep)}. This signal is unsymmetrical and comparable to those of the catecholate and tironate bis complexes. Also similar to the {Fe(cat)$_2$} and {Fe(tiron)$_2$} spectra, {Fe(pep)$_2$} displayed splitting of the $g = 4.22$ signal, shown more conspicuously in the expansion provided in Figure 6b. A weak signal at $g \approx 1.98$ was also observed.

[Fe(pep)$_3$]$^{3-}$. The tris-peptide model complex, [Fe(pep)$_3$]$^{3-}$, exhibited a spectrum similar to those of the [Fe(cat)$_3$]$^{3-}$ and [Fe(tiron)$_3$]$^{9-}$ complexes with a typical rhombic hs-Fe^{3+} signal, centered at $g = 4.23$, with a wing down to $g \approx 9$ (Figure 6a). When compared to the $g = 4.22$ signal of {Fe(pep)$_2$}, this tris signal revealed no splitting. The intensity at $g = 4.23$ was greater than for either the mono- or bis-peptide complexes, a situation similar to that found for the catecholate compounds.

Simulations of Anaerobic {Fe(pep)$_n$} ($n = 1-3$) Peptide Spectra. {Fe(pep)}. The spectrum of the 1:1 complex for iron peptide (Figure 6) is quite different than that of the 1:1 complex of iron and catecholate (Figure 1). While the features at $g = 8.1$, 5.5, and 4.3 are still seen, they are much more diffuse. The most significant difference is a sharp feature at $g = 2$ that has long tails on each side. Spectra with features both at $g = 4.3$ and $g = 2$ have been observed for iron in glassy states where the D-strain and average value of D are such that there are sites that are near the low-field limit, as well as those near the high-field limit.[46] In the high-field limit, the spectrum will now be centered around the true g value, that is, $g = 2$. Figure 7 shows several simulations for $\lambda = 0.15$ for various values of D_0. When D/h is greater than the microwave frequency (9.0 GHz or 0.3 cm^{-1}), a spectrum with features at $g = 8.1$, 5.5, and 4.3 that is similar to that for the 1:1 complex of iron and catecholate is observed. If the value of D_0 is decreased below the microwave frequency, the features at $g = 8.1$, 5.5, and 4.3 become weaker and more diffuse and a broad feature(s) around $g = 2$ appears. As D is further decreased, the center of the broad feature(s) at $g = 2$ sharpens. This feature is due to the $m_s = -1/2$ to 1/2 transition; the other four fine structure transitions will also contribute in the limit that D goes to zero. While the simulation with $D_0 = 0.15$ (Figure 7d) gives a reasonable fit to the experimental spectrum, the $g = 4.3$ feature is much broader than that seen in the experimental spectrum. The fit could be improved if a contribution from a second distribution with $D_0 = 0.44$ and $\lambda = 0.24$ was added in a 5:1 ratio. Because the distribution patterns significantly overlap each other, it is difficult to ascertain if the second distribution arises from a chemically distinct species or if our choice of distribution function does not accurately describe the actual distribution of D and E for the 1:1 complex. The simulation reproduces the features in the experimental spectrum quite well, except that simula-

(62) Waite, J. H. *Int. J. Biol. Macromol.* **1990**, *12*, 139−143.
(63) Smith, J. J.; Thomson, A. J.; Proudfoot, A. E. I.; Wells, T. N. C. *Eur. J. Biochem.* **1997**, *244*, 325−333.
(64) Taylor, S. W.; Luther III, G. W.; Waite, J. H. *Inorg. Chem.* **1994**, *33*, 5819−5824.

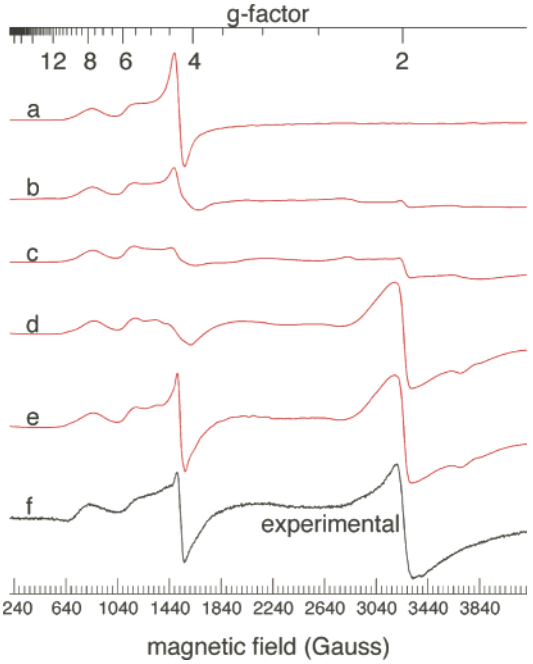

Figure 7. Simulated and experimental spectra of Fe(pep). (a−d) Simulated spectra with differing values of D_0 but keeping E_0/D_0 ($\lambda = 0.15$), $\Delta D/D$, and $\Delta E/E$ constant; parameters as listed in Table 1. (a) $D_0 = 0.63$ cm^{-1}. (b) $D_0 = 0.32$ cm^{-1}. (c) $D_0 = 0.24$ cm^{-1}. (d) $D_0 = 0.16$ cm^{-1}. (e) Same as (d) except with an addition of a second minor species (4:1 ratio) with $D_0 = 0.44$ cm^{-1} $\lambda = 0.24$; other parameters as in Table 1. (f) Experimental.

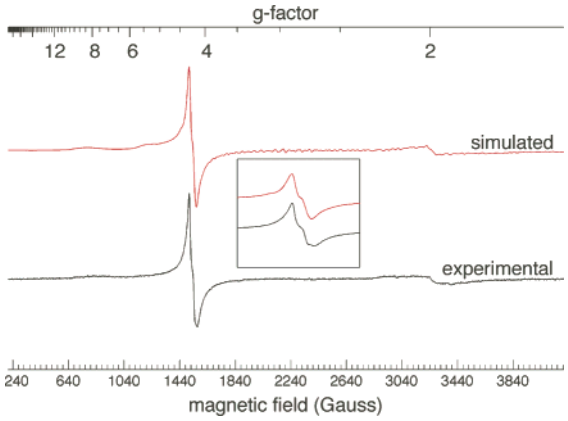

Figure 8. Simulated and experimental spectra of Fe(pep)$_2$. Inset shows $g = 4$ region at higher resolution.

tion predicts a weak feature at $g = 1.75$ on the high-field tail of the $g = 2$ feature, which is not seen in the experimental spectrum.

Aside from the much smaller values of D_0 and E_0, the 1:1 peptide spectrum differs in that a much smaller correlation coefficient between D and E is needed. Not only is it smaller than those of any of the three catecholate complexes but also it is opposite in sign. This suggests that the origin of the strain in the 1:1 peptide complex is more complicated than for the catecholate complexes and may arise from multiple sources. The ratio of D_0 and E_0 of 0.15 is similar to that for the 1:1 catecholate complex implying that the 1:1 peptide complex is indeed a 1:1 complex.

{Fe(pep)$_2$}. The spectrum of the 1:2 iron peptide complex, which is shown in Figure 8, is dominated by a $g = 4.3$ feature which shows a 25 G splitting. While the spectrum is very

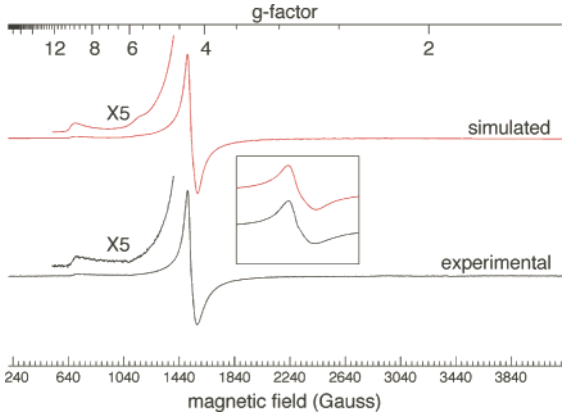

Figure 9. Simulated and experimental spectra of Fe(pep)$_3$. Inset shows $g = 4$ region at higher resolution.

similar to that of the 1:2 iron catecholate complex, there are a couple of differences. First, the $g = 8.3$ and 5.6 features are more diffuse, and second is the appearance of a weak but distinct feature at $g = 2$. Simulation showed that the experimental spectrum could be well accounted for with a double distribution. The major component has D_0 and λ values that are similar to those for the 1:2 catecholate complex. The minor second component has D_0 and λ values similar to the major component in the 1:1 peptide complex. As the distributions for the two components overlap, it may be that the correct distribution of D and E for the 1:2 complex is so large that it includes sites where D is close to zero. However, because the values of D_0 and λ for the second component are similar to those for the primary component for the 1:1 complex, it is more likely that there is some 1:1 complex present in the putatively 1:2 complex and vice versa. Each of the compounds discussed in this paper were generated from base addition to solutions of metal and ligand. As discussed previously, each compound was considered fully formed when UV−vis absorption changes maximized during a titration.[39,40] However, we cannot rule out the possibility of incomplete formation for any given complex.

[Fe(pep)$_3$]$^{3-}$. The spectrum of the 1:3 peptide complex, which is shown in Figure 9, is very similar to that of the 1:3 catecholate complex. The values of D and E are, within experimental error, the same for both systems. The only significant difference between the two is that the residual line width for the catecholate complex is greater than that for the peptide complex.

Spectra of Aerobic {Fe(cat)$_n$} ($n = 1-3$) Catecholate Complexes. Thus far we have examined only samples prepared anaerobically. Marine mussels often synthesize their glues in the turbulent and aerated waters of the intertidal zone. We wish to compare spectra of these iron complexes in the presence and absence of oxygen. The compounds described below were prepared in air. The descriptions below focus on differences in the anaerobic versus aerobic complexes.

{Fe(cat)}. For the aerobic mono-catecholate sample, {Fe(cat)}, we found a spectrum similar to that seen under anaerobic conditions with hs-Fe^{3+} peaks at $g = 8.05$, 5.50, and 4.24. The intensity of this highly strained rhombic ($\lambda =$

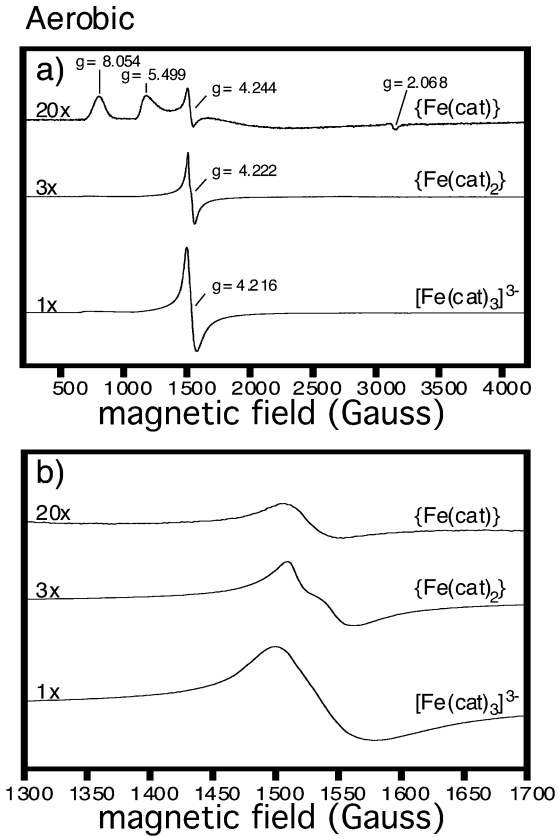

Figure 10. EPR spectra of aerobic iron(III)−catecholate complexes of (a) the full spectral region and (b) an expansion of the $g \approx 4.2$ signal only. The vertical scales of each spectrum are adjusted as labeled to allow comparisons.

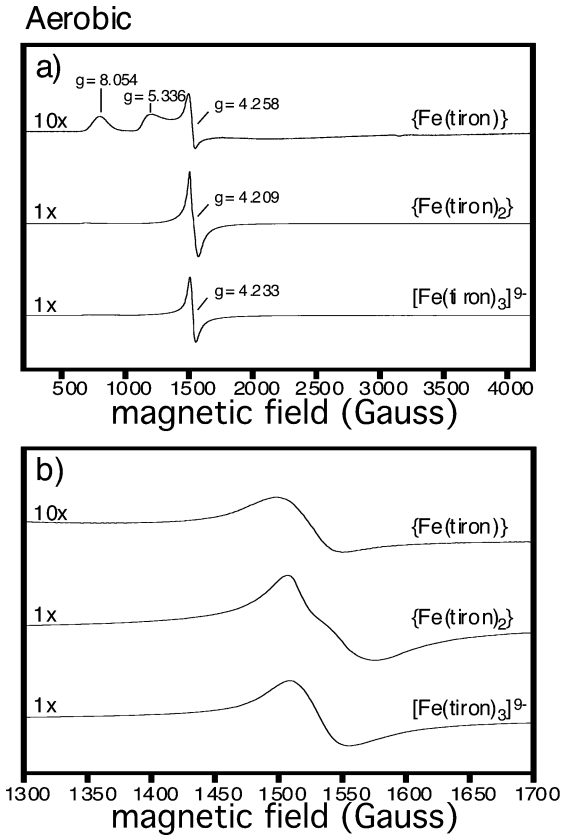

Figure 11. EPR spectra of aerobic iron(III)−tironate complexes of (a) the full spectral region and (b) an expansion of the $g \approx 4.2$ signal only. The vertical scales of each spectrum are adjusted as labeled to allow comparisons.

0.12) hs-Fe^{3+} spectrum was weaker than that occurring under anaerobic conditions, and a new feature at $g = 2.068$ was seen (Figure 10a).

{Fe(cat)$_2$}. Aerobically prepared {Fe(cat)$_2$} samples showed spectra that were similar to those prepared anaerobically. While the feature at $g \approx 8.1$ was observed, that at g ≈ 5.5 was not (Figure 10a). The $g \approx 8$ feature in this spectrum was less intense than that seen in the complimentary anaerobic sample of {Fe(cat)$_2$}, while the $g = 4.24$ signal intensity was significantly greater, suggesting some small change in the magnitude of the *D*- and *E*-strain. No evidence was seen for a signal in the $g \approx 2.0$ region.

[Fe(cat)$_3$]$^{3-}$. The EPR spectrum of [Fe(cat)$_3$]$^{3-}$, which is very similar to that of the anaerobic counterpart (Figure 10a), was dominated by a $g = 4.22$, which is better shown in Figure 10b, indicating that like the anaerobic system λ is close to 1/3.

Spectra of Aerobic {Fe(tiron)$_n$} ($n = 1-3$) Tironate Complexes. Spectra taken of aerobically prepared {Fe(tiron)}, {Fe(tiron)$_2$}, and [Fe(tiron)$_3$]$^{9-}$ (Figure 11) were all similar to those seen under anaerobically prepared conditions (Figure 5). For the aerobic {Fe(tiron)} spectrum, a very weak signal at $g \approx 2.0$ is seen. Unlike the anaerobically prepared bis sample, aerobic {Fe(tiron)$_2$} showed a well-defined splitting of the $g \approx 4.22$ feature, seen in Figure 11b.

Spectra of Aerobic Mono, Bis and Tris Fe−Peptide Complexes. {Fe(pep)}. The EPR spectrum of aerobic, mono {Fe(pep)} (Figure 12) appeared quite different than that of anaerobic {Fe(pep)} (Figure 6). This aerobic spectrum showed hs-Fe^{3+} signals at $g = 7.62$ and 4.35. The $g = 4.3$ resonance was significantly broader than the anaerobic counterpart (Figure 6b) with the $g = 5.4$ feature being no longer resolved. These results suggest that there are small but significant differences in the distribution of *D* and *E* values between the anaerobic and aerobic samples. A major change occurred in the $g \approx 2.0$ region of the spectrum for this sample. Whereas in anaerobic {Fe(pep)} we observed one highly unsymmetrical signal, which results from hs-Fe^{3+} sites with values of *D* smaller than the microwave frequency, here with aerobic {Fe(pep)} we found the region split into two distinct features. The first of these signals occurred at $g = 2.08$ and the second was at $g = 1.96$. The $g = 1.96$ arises from hs-Fe^{3+} sites with small values of *D*, while the origin of the $g \approx 2$ signal is not clear. Possibilities include low-spin Fe^{3+} or iron−iron coupling.[9,52,65−67]

{Fe(pep)$_2$}. The EPR spectrum of aerobically prepared {Fe(pep)$_2$} exhibited characteristics much like those of the anaerobic sample. The spectrum in Figure 12a is dominated by a signal at $g = 4.24$ with a wing stretching down to a broad peak around $g \approx 8$. Splitting was again apparent in the $g = 4.24$ peak (Figure 12b). Weak signal(s) were also observed between $g \approx 2.2$ and 1.9. The $g = 1.9$ signal is similar to those seen in the anaerobically prepared {Fe(pep)$_2$} and probably also arises from sites which have very small values of *D* and *E*.

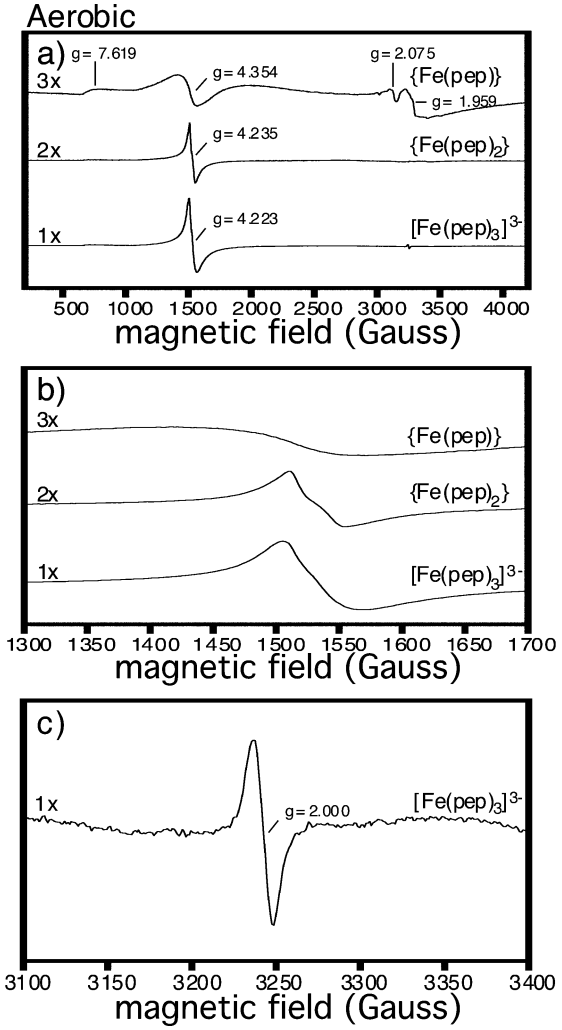

Figure 12. EPR spectra of aerobic iron(III)−AdopaTP complexes of (a) the full spectral region, (b) an expansion of the $g \approx 4.2$ signal only, and (c) an expansion of the organic radical region in $[Fe(pep)_3]^{3-}$. The vertical scales of each spectrum are adjusted as labeled to allow comparisons.

$[Fe(pep)_3]^{3-}$. The spectrum for the aerobic $[Fe(pep)_3]^{3-}$ complex, shown in Figure 12a, appeared quite similar to the anaerobic counterpart. The $g = 4.22$ signal was slightly sharper and more intense then the same signal in the anaerobic spectrum. Another difference was the appearance of a small, sharp signal at $g = 2.000$, which is expanded in Figure 12c. This signal was not present in the anaerobic counterpart. The narrow width and location of this signal are both characteristic of organic radicals.[68−74] Furthermore, growth of this $g = 2.000$ signal in air coincides with a loss of hs-Fe^{3+} intensity relative to this same sample when anaerobic. Control solutions of the peptide in base, but without any iron, did not display the clear presence of a radical species.

Discussion

Examination of EPR spectra for the anaerobic Fe−catecholate model complexes showed sufficient differences to distinguish among the mono, bis, and tris binding modes. The $g \approx 4.3$ hs-Fe^{3+} signal became progressively more intense during the progression from mono to bis to tris compounds. For example, the three catecholates of $[Fe(cat)_3]^{3-}$ yielded the most intense $g \approx 4.3$ resonance, whereas for the mono species {Fe(cat)}, the smallest signal was observed in this region. In general, simulations showed that differences in these spectra could be attributed to differences in the rhombic character of the zero-field tensor (D), with the rhombic character ($\lambda = E/D$) increasing in the series mono < bis < tris. Simulations also showed that the spectra for the Fe−catecholate and Fe−tironate samples could be explained in terms of a single hs-Fe^{3+} species having a broad distribution of D and E values. These spectra are typical of hs-Fe^{3+} in which the magnitude of the zero-field tensor is greater than that of the microwave frequency (ν).

EPR spectra of the peptide complexes were generally similar to both the analogous catecholate and tironate samples with regard to hs-Fe^{3+} signals. The same splitting patterns and general arrangement of signals were observed in all bis and tris samples, indicating a similarity in the rhombic character (E/D), as well the magnitude of strain in D and E, among the catecholate, tironate, and peptide samples for these two coordination environments. The intensity and shape of features in {Fe(pep)}, however, were less well defined than those of {Fe(cat)} and {Fe(tiron)}.

The most significant difference between the catecholate and peptide spectra is the appearance of a 1:1 complex for which a large portion of the distribution contains a significant number of sites outside of the low field-limit, that is, the appearance of a $g = 1.9$ peak resulting from sites having low values of D and E. In the 1:1 complexes, the coordination sphere is most likely completed by bound solvent (water or hydroxide). In the case of the peptide complex, weak coordination to other groups on the peptide could also occur and this binding may give rise to the atypical values of D_0 and E_0. To bring about these low values of D_0 and E_0, the symmetry around the iron would have to be closer to octahedral or the strength of the ligand field reduced. The bis and tris catecholate and peptide species were much more similar. Also, unlike the Fe−catecholate or Fe−tironate complexes, simulation of the mono and the bis peptide spectra required the use of two separate distributions of D and E values, suggesting the presence of two distinct species.

Of the EPR spectra observed for the catecholate, tironate, and peptide complexes prepared under an inert atmosphere,

(65) Sakurai, H.; Tsuchiya, K.; Migita, K. *Inorg. Chem.* **1988**, *27*, 3877−3879.
(66) Zhilinskaya, E. A.; Delahay, G.; Mauvezin, M.; Coq, B.; Aboukais, A. *Langmuir* **2003**, *19*, 3596−3602.
(67) Palmer, G. In *Physical Methods in Bioinorganic Chemistry: Spectroscopy and Magnetism*; Que, L., Jr., Ed.; University Science Books: Sausalito, CA, 2000.
(68) Felix, A. M.; Winter, D. P.; Wang, S.-S.; Kulesha, I. D.; Pool, W. R.; Hane, D. L.; Sheppard, H. *J. Med. Chem.* **1974**, *17*, 422−426.
(69) Felix, C. C.; Sealy, R. C. *J. Am. Chem. Soc.* **1981**, *103*, 2831−2836.
(70) Herebian, D.; Bothe, E.; Bill, E.; Weyhermuller, T.; Wieghardt, K. *J. Am. Chem. Soc.* **2001**, *123*, 10012−10023.
(71) Magers, K. D.; Smith, C. G.; Sawyer, D. T. *Inorg. Chem.* **1980**, *19*, 492−496.
(72) Merdy, P.; Guillon, E.; Frapart, Y.-M.; Aplincourt, M. *New J. Chem.* **2003**, *27*, 577−582.
(73) Pierpont, C. G.; Buchanan, R. M. *Coord. Chem. Rev.* **1981**, *38*, 45−87.
(74) Stubbe, J.; van der Donk, W. A. *Chem. Rev.* **1998**, *98*, 705−762.

the tris species showed the greatest rhombic character relative to the mono and bis analogues. Splitting of the anaerobic and aerobic hs-Fe^{3+} signals of the bis-coordinated samples may prove to be a characteristic spectral feature useful for identification of this coordination environment in biological samples. Consequently, these model spectra show that distinct features can be found among the coordination modes examined. In the case of adhesive plaques isolated from live mussels, we found a relatively simple spectrum predominated by a $g \approx 4.2$ signal.[13] We can now say with more confidence that the plaque spectrum is that of a tris $[Fe(DOPA)_3]^{3-}$ complex. Furthermore, $[Fe(pep)_3]^{3-}$ appears to be the predominant observable Fe^{3+} species contained in mussel adhesive plaques.

When comparing either iron(III)−catecholate or iron(III)−tironate samples generated anaerobically versus in air, both preparation methods yielded complexes with similar EPR spectral characteristics. By contrast, the Fe−peptide complexes brought to light some interesting differences when comparing the samples prepared in air versus under an inert atmosphere with regard to formation of organic radicals. A radical was observed for the $[Fe(pep)_3]^{3-}$ complex prepared in air but not the analogous $[Fe(cat)_3]^{3-}$. These results are consistent with an earlier report in which no radical was observed in the analogous tris catecholate complex $[Fe(cat)_3]^{3-}$.[14] Neither {Fe(pep)} nor $\{Fe(pep)_2\}$ formed a radical when prepared aerobically. The radical signal in the tris peptide complex was weak. This lack of intensity may indicate that formation of the radical species is low or that subsequent reactivity such as radical−radical coupling may have decreased the observable resonance. In contrast to anaerobic samples, these results indicate that aerobic iron−catecholate complexes do not provide suitable models for DOPA-containing biological models. If $[Fe(cat)_3]^{3-}$ was taken to be a good model for $[Fe(DOPA)_3]^{3-}$, the oxygen reactivity might have been missed.

Interestingly, a radical was also observed in iron- and DOPA-rich whole adhesive plaques taken from live mussels at $g = 1.997$.[13] Thus, an $[Fe(DOPA)_3]^{3-}$ species and oxygen appear to be required for radical generation in this biological material. At this time, the identity of these radicals is unknown. Although valence tautomerism processes can directly generate ligand-based radicals,[24,73] we disfavor such an assignment given that oxygen is required to form this radical. Perhaps a multistep process is at hand in which an Fe^{3+}−catecholate species can first undergo valence tautomerism to yield an Fe^{2+}−semiquinone. Subsequent reaction of this oxidized ligand with O_2 may then generate an oxygenated and radical-bearing ligand. However, we do not observe any significant radical in anaerobic $[Fe(pep)_3]^{3-}$, thus disfavoring the initial valence tautomerism. A similar valance tautomerism process was proposed to take place for intradiol catechol dioxygenases.[15,28] A possible mechanism of action for this enzyme involves catechol binding to an Fe^{3+} center followed by valence tautomerism to an Fe^{2+}−semiquinone.[15,28] Reaction with oxygen then yields a ligand-based peroxy radical.[15,28] Prior to oxygen exposure, model complexes of this enzyme active site displayed no radical species by EPR spectroscopy.[15,28] More work must be performed in order to identify the origin and identity of such radical species in enzymes and biological materials.

Conclusions

The EPR spectra of iron bound by catecholate, tironate, and the AdopaTP peptide in mono, bis, and tris coordination environments have been presented. These spectra may provide useful data for identification of bonding motifs in biological systems. Such models of potential metal−protein interactions allow comparisons with data collected from marine mussels. Prior studies showed that adhesive plaques and an iron cross-linked protein solid both contained an organic radical. Data presented here indicate that $Fe(DOPA)_3$ moieties and oxygen are required to generate such radical species. Protein-based radicals may provide a route to radical−radical coupling for the generation of organic cross-links or protein−surface binding for the creation of surface bonding.

Acknowledgment. We thank Joshua Telser for valuable discussions. J.J.W. is grateful for support of this work provided by an Arnold and Mabel Beckman Foundation Young Investigator Award, a National Science Foundation Faculty Early Career Development (CAREER) Award, the Purdue Research Foundation, an Alfred P. Sloan Foundation Research Fellowship, and the Lord Corporation.

IC060685P